Supporting Information

ZnO Nanocluster-Functionalised Single-Walled Carbon Nanotubes Synthesized by Microwave Irradiation for Highly Sensitive NO_2 detection at Room Temperature

Suyoung Park,[†] Youngmin Byoun,[⊥] Hyoungku Kang,[‡] Young-Jun Song,[*,§] Sun-Woo Choi[*,§]

[†]Department of Aviation Maintenance Engineering, Far East University, Eumseong-gun, Chungcheongbuk-do 27601, Republic of Korea

[⊥]Metal & Machinery Team, Korea Conformity Laboratories (KCL), Seoul 08503, Republic of Korea

[‡]Department of Electrical Engineering, Korea National University of Transportation, Chungju-si, Chungcheongbuk-do 27469, Republic of Korea

[§]Department of Materials Science and Engineering, Kangwon National University, Samcheok-si, Gangwon-do 25912, Republic of Korea

* Corresponding authors.
E-mail: yjsong64@kangwon.ac.kr (Y.-J. Song), csw0427@kangwon.ac.kr (S.-W. Choi)

• Calculation of detection limit (DL)[equation S1, S2]

1. As shown in Fig. S1(a), the slope value (~ 0.552) and the value of goodness-of-fit (R^2, ~ 0.98) were derived from the response values versus NO_2 concentration of the fabricated sensor.

2. Before NO_2 gas injected in the gas chamber, we have taken resistance points of $N = 11$ at the base line.

3. As shown in Fig. S1(b), We have plotted the data (resistance value versus time) and then a 5th order polynomial fit is performed within data-point range (see Table S1).

4. To obtain the theoretical detection limit (DL), the root-mean squared deviation (RMS_{noise}) has been calculated as follows,

$$RMS_{noise}(ppm^{-1}) = \sqrt{V_{x^2}/(N-1)} \text{ , where } V_{x^2} = \sum(Y_i - Y)^2 \qquad \text{(equation S1)}$$

Where Y_i is the measured resistance value and Y is the corresponding value calculated from the curve-fitting equation. The DL value could be finally calculated using the following equation.

$$\text{Detection limit (DL)} = 3 \times \frac{RMS_{noise}}{slope} \qquad \text{(equation S2)}$$

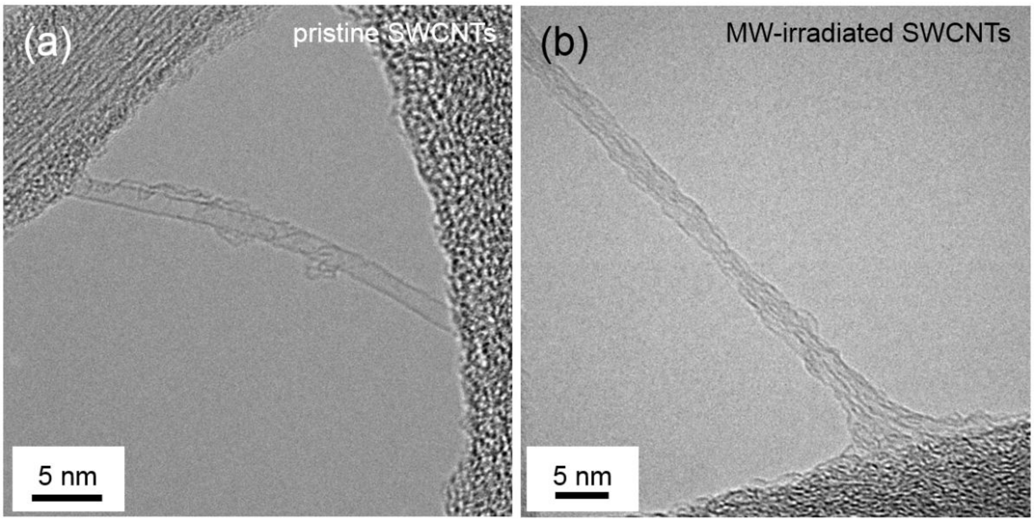

Figure S1. High-resolution TEM images of (a) pristine and (b) MW-irradiated SWCNTs.

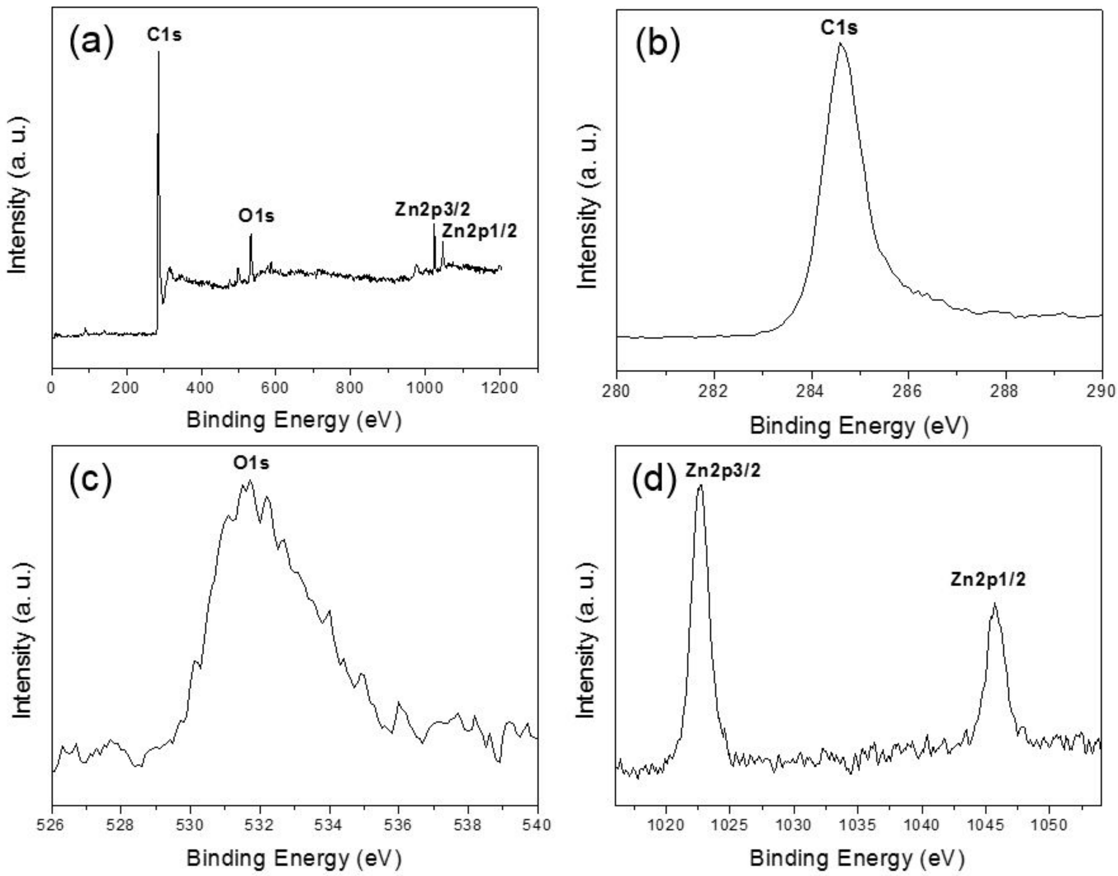

Figure S2. XPS results of the Z-SWCNTs: (a) survey-scanned XPS spectrum of Z-SWCNTs, core level XPS spectra of (b) C 1s, (c) O 1s and (d) Zn 2p.

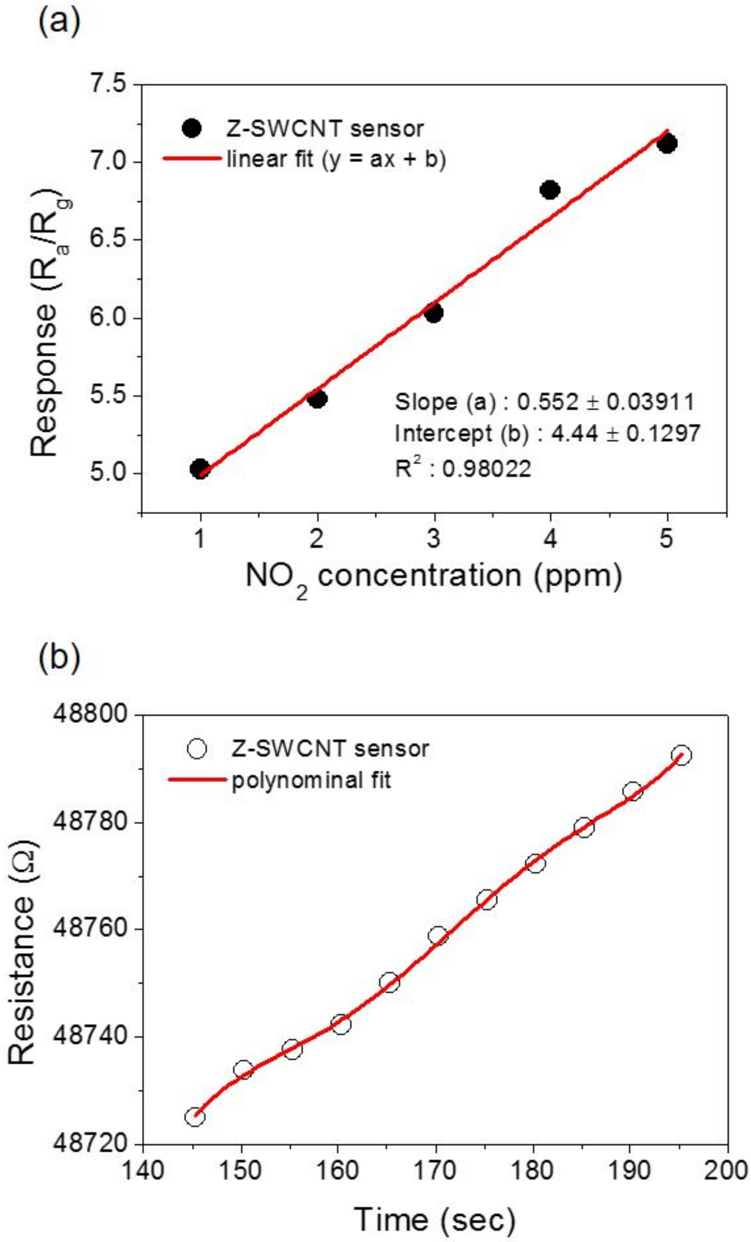

Figure S3. Fitting plots of Z-SWCNT sensor: (a) linear fitting, (b) 5th order polynomial fitting.

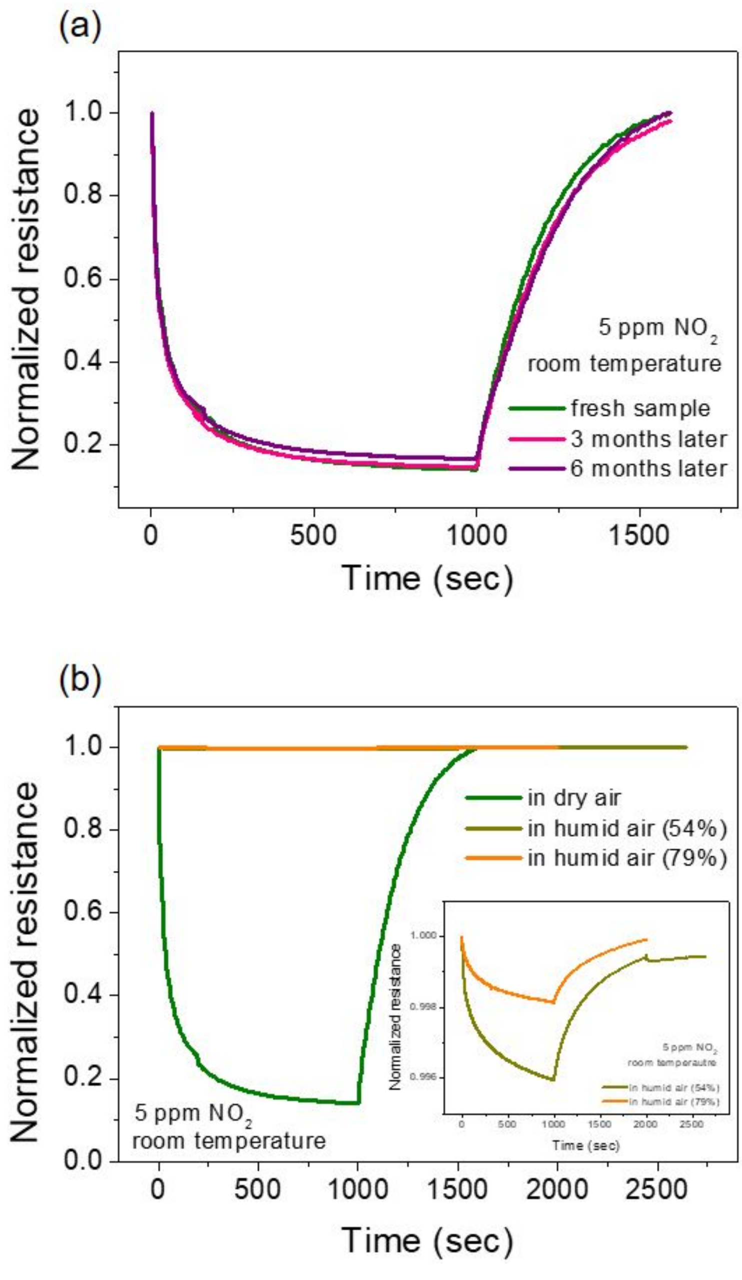

Figure S4. (a) Long-term stability of the Z-SWCNTs, and (b) comparison of the NO_2 response of Z-SWCNTs under dry air, RH 54% and RH 79% humid air, respectively.

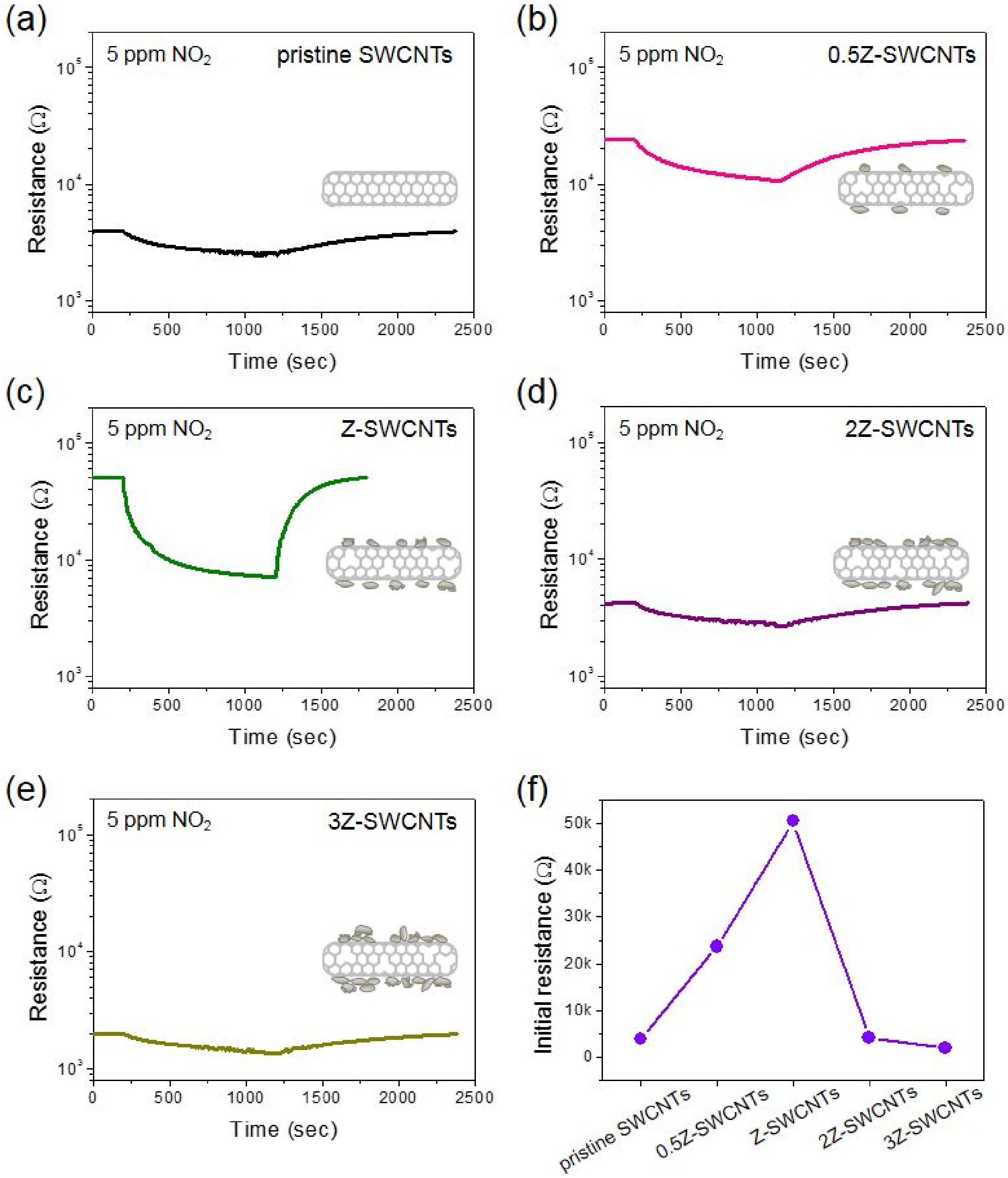

Figure S5. Resistance curves of the *n*-ZnO NC-functionalised defect-induced SWCNTs: (a) pristine SWCNTs, (b) 0.5Z-SWCNTs, (c) Z-SWCNTs, (d) 2Z-SWCNTs, and (e) 3Z-SWCNTs. (d) Initial resistance values of each sensor. (f) Summary of initial resistance values of the fabricated sensors.

Table S1. Polynomial fitting data of the Z-SWCNT sensor

Time (sec)	$(Y_i - Y)$	$(Y_i - Y)^2$
145	0.0101	0.000102
150	-0.00508	2.58×10^{-5}
155	-0.00616	3.79×10^{-5}
160	-0.00024	5.76×10^{-8}
165	-0.00052	2.7×10^{-7}
170	-0.0496	0.00246
175	-0.00068	4.62×10^{-7}
180	-0.00076	5.78×10^{-7}
185	0.0002	4.8×10^{-8}
190	-2×10^{-5}	4×10^{-10}
195	-1×10^{-5}	1×10^{-10}

Table S2. Comparison of NO_2-response in Z-SWCNT sensor with various types of sensors prepared different sensing materials

Materials	Concentration (ppm)	Temperature (^oC)	Gas response	Reference
Z-SWCNTs	1	RT	5.03 (R_a/R_g)	this work
Z-SWCNTs	1	RT	403% ($\Delta R/R_a$)×100	this work
Cu_2O-conjugated RGO*	2	RT	67.8% ($\Delta I/I_a$)×100	1
SnO_2-ZnO core-shell NWs	1	RT	238.73% ($\Delta R/R_a$)×100	2
Co_3O_4-intercalated RGO	60	RT	80% ($\Delta R/R_a$)×100	3
PPy** thin films	10	RT	12% ($\Delta R/R_a$)×100	4
ZnO-RGO hybrid	5	RT	25.6% ($\Delta R/R_a$)×100	5
rGO-CNT-SnO_2 hybrid	5	RT	2.53 (R_a/R_g)	6
Mesoporous NiO nanosheets	5	RT	0.30 ($\Delta G/G_a$)	7
TeO_2-SnO_2 heterostructure	3	RT	9.97 (R_a/R_g)	8
Bi-layer graphene	5	RT	12.87% ($\Delta R/R_a$)×100	9

* rGO: Reduced graphene oxide, ** PPy: Polypyrrole,

References

(1) Deng, S.; Tjoa, V.; Fan, H. M.; Tan, H. R.; Sayle, D. C.; Olivo, M.; Mhaisalkar, S.;

Wei, J.; Sow, C. H. Reduced graphene oxide conjugated Cu_2O nanowire mesocrystals for high-performance NO_2 gas sensor, *J. Am. Chem. Soc.* **2012**, *134*, 4905–4917.

(2) Park, S.; An, S.; Mun, Y.; Lee, C. UV-enhanced NO_2 gas sensing properties of SnO_2-Core/ZnO-shell nanowires at room temperature, *ACS Appl. Mater. Interfaces* **2013**, *5*, 4285–4292.

(3) Chen, N.; Li, X.; Wang, X.; Yu, J.; Wang, J.; Tang, Z.; Akbar, S. A. Enhanced room temperature sensing of Co_3O_4-intercalated reduced graphene oxide based gas sensors, *Sens. Actuators B: Chem.* **2013**, *188*, 902–908.

(4) Navale, S. T.; Mane, A. T.; Chougule, M. A.; Sakhare, R. D.; Nalage, S. R.; Patil, V. B. Highly selective and sensitive room temperature NO_2 gas sensors based on polypyrrole thin films, *Synthetic Met.* **2014**, *189*, 94–99.

(5) Liu, S.; Yu, B.; Zhang, H.; Fei, T.; Zhang, T. Enhancing NO_2 gas sensing performances at room temperature based on reduced graphene oxide-ZnO nanoparticles hybrids, *Sens. Actuators B: Chem.* **2014**, *202*, 272–278.

(6) Liu, S.; Wang, Z.; Zhang, Y.; Zhang, C.; Zhang, T. High performance room temperature NO_2 sensors based on reduced graphene oxide-multiwalled carbon nanotubes-tin oxide nanoparticles hybrids, *Sens. Actuators B: Chem.* **2015**, *211*, 318–324.

(7) Zhang, J.; Zeng, D.; Zhu, Q.; Wu, J.; Huang, Q.; Xie, C. Effect of nickel vacancies on the room-temperature NO_2 sensing properties of mesoporous NiO nanosheets, *J. Phys. Chem. C* **2016**, *5*, 3936–3945.

(8) Yeh, B.-Y.; Huang, P.-F.; Tseng, W. J. Enhanced room-temperature NO_2 gas sensing with TeO_2/SnO_2 brush- and bead-like nanowire hybrid structures, *Nanotechnology* **2017**, *28*, 045501.

(9) Seekaew, Y.; Phokhaatkul, D.; Wisitsoraat, A.; Wongchoosuk, C. Highly sensitive and selective room-temperature NO_2 gas sensor based on bilayer transferred chemical vapor deposited graphene, *Appl. Surf. Sci.* **2017**, *404*, 357–363.